Variable Range Hopping in SrTiO$_3$−Ca$_{10}$(PO$_4$)$_6$(OH)$_2$ Bio-Ceramic Composites

Apurba Das and Pamu Dobbidi*

Read Online

ACCESS | Metrics & More | Article Recommendations | Supporting Information

ABSTRACT: We investigate the electrical properties in ceramics, focusing primarily on the conductivity mechanisms crucial to bio-electrets' service life. A biocompatible ceramic composite of varying concentrations of SrTiO$_3$ (ST) and Ca$_{10}$(PO$_4$)$_6$(OH)$_2$ (HAP) is developed. By X-ray diffraction, we establish the microstructural and phase evolution of the bio-composites. The crystallite sizes are found to increase with the increasing concentration of ST in the composites. The composites' micrograph reveals the presence of pores, and the grain sizes calculated from it are found to follow a trend similar to the crystallite size. The conduction mechanisms in the composites are studied to explore the composites' electrical properties from the perspective of biological applications. The conductivity is very low ($\simeq 10^{-8}$ S/cm), and the porous structure of the composites revealed from the micrographs is one of the factors for such low conductivity. From a plethora of conduction mechanisms, Motts' variable range hopping (VRH) conduction is projected as the most appropriate mechanism that appropriately describes the conduction process in the composites. Motts' VRH is also related to the polarization mechanism associated with the development of electrets. Our study points toward the practical potential of applying the designed bio-composites in generating bio-electrets or understanding the electrical properties that are at the forefront of research in designing electro-active smart scaffolds for bone tissue engineering applications.
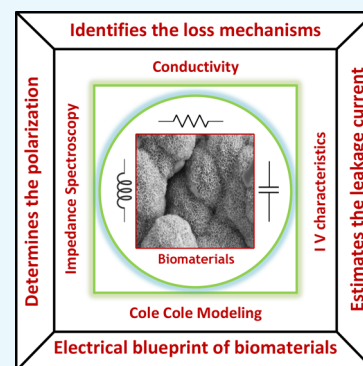
INTRODUCTION

The design of novel bio-ceramics to augment the need for faster healing responses has been in the limelight of biomedical research in the last few decades.[1] For years, clinicians have recognized the role of electrical stimulation in promoting bone healing and regeneration.[2] Such applications of external stimulations have become a preferred course of treatment for faster healing of fractures. Additionally, bone tissue engineering primarily relies upon the scaffolds to restore the missing bone volume.[3] The success of scaffolds in clinical settings depends on the materials chosen to develop the scaffold template. Biomaterials research has predicted the suitability of electrically active bioceramics for tissue engineering applications.[4] For instance, scaffolds fabricated of ceramics displaying high permittivity have the capacity of undergoing a high degree of polarization when they are implanted in *in vivo* settings, and electrical stimulation is applied to the injured site.[5] As the application of external electrical stimulation has become increasingly ubiquitous in medical science, electro-active scaffolds can provide reliable platforms to augment the process. These electro-active scaffolds would continue producing the electric field *in vivo* (by dint of polarization) even after the removal of the external stimulation. Thus, the polarized electric field (PEF) will contribute to an expedited healing process and are quite desirable for faster and enhanced bone regeneration.[5]

It is a well-established phenomenon that when an electric field is applied to dielectric materials (such as bio-ceramics),

the dipoles will align themselves in the direction of the field.[5] Once the field is removed, the dipoles attempt to revert to their original state. The ease of undergoing polarization and the rapidity with which the dipoles move back to their original state mostly depends on the specimens' conduction mechanism.[6] Higher permittivity is associated with higher loss. Therefore, the lower conductivity specimens are beneficial for longer retention of the polarization and are essential from a biomedical perspective. Choosing a material for designing scaffolds must be preceded by a thorough investigation of its electrical permittivity and understanding its loss mechanisms. The elegant framework of impedance spectroscopy is a vital tool for extracting such properties and is slowly gaining its edge in biomaterials research.[7] Impedance analysis (specifically the conduction mechanisms) can shed light on the phenomenon of hopping conduction, which is identified as the major contributor to the depletion of PEFs' strength[6] (a schematic description of the hopping process is included in Figure 1). The dielectric constant (ϵ_r) largely determines the biomaterials' capacity to store charges in them. However, the presence
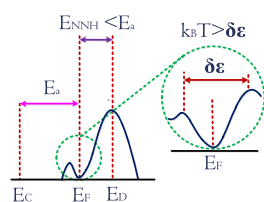
Figure 1. Schematic illustration of the various conduction mechanisms. E_F represents the Fermi level, E_C represents the edge of the conduction band, and E_D is the energy level of an isolated donor. The double arrow represented in magenta is the thermally active band conduction, expressed by an equation of the type $\rho = \rho_0 \exp(E_a/k_B T)$. The double arrow in purple represents the nearest neighbor hopping conduction, expressed by $\rho = \rho_0 \exp(E_{NNH}/k_B T)$. Finally, the double arrow in red represents the Mott's variable range hopping (VRH) conduction, expressed by $\rho = \rho_0 \exp(T_0/T)^{1/4}$. The thermally activated band conduction process have activation energy greater than the nearest neighbor hopping conduction. The hopping transport usually takes place amongst the localized states, which are near to the Fermi level.

of relaxations in ceramics displays the need to identify an appropriate frequency of operation along with the knowledge of conduction mechanisms active within the specimens.[8] To maximize the PEF in *in vivo* settings, the ϵ_r of the composite material should be higher.[5] Additionally, the frequency of external stimulation is to be in line with the scaffold materials' ϵ_r, which has to be chosen so that the dipolar relaxations are minimum.[5] It was pointed out previously that ceramics with higher ϵ_r have higher losses in terms of polarization. Optimum balancing by a detailed study of the loss mechanisms (conduction) is of paramount importance under that scenario. Apart from the scaffolds, bio-electrets are an emerging key player in transdermal drug delivery and self-healing bandages. Its application largely hinges on the amount of charge that can be retained on their surfaces.[9] These surface charges generate electric fields and micro-currents that lead to faster wound healing. The usability of an electret is dependent on the time to which it can retain its surface charge. Hence, the conduction processes in the prepared ceramics play a significant role in determining their service lifetime.[10,11]

$Ca_{10}(PO_4)_6(OH)_2$ (HAP) exhibits excellent bio-compatibility, and its electrical properties are not explored entirely.[12] $SrTiO_3$ (ST) has recently been considered for biomedical applications, and the preliminary results have been quite inspiring.[13] A study by Xin *et al.*[13] concluded that the ST nanotube array fabricated over Ti could serve as a platform for effective release of Sr ions that promotes osseointegration. Such nanotube array could effectively induce precipitation of apatite from simulated body fluid demonstrating the superior bioactivity of the nanotubes. In another study, $ST-TiO_2$ nanoparticle-nanotube heterostructures were fabricated over Ti implants, and the effect of Sr release on the cell proliferation behavior of SaOS2 cells was studied.[14] The study indicated that Sr release up to 3 ppm displayed superior biological properties, and above that limit (3 ppm), the SaOS2 cells were adversely affected. A study on a composite of HAP and ST was considered for understanding the mechanical properties, and it revealed that a composite (50 wt % ST and 50 wt % HAP) displayed superior elastic modulus than HAP (54 ± 4 GPa for the composite in comparison to 46 ± 10 GPa for HAP).[15] In biomedical applications, ST can serve as an important platform for the release of Sr ions, and medical research has explicitly shown that Sr ions can effectively prevent bone loss.

Administering doses of Sr ions *via* "SrRan" drug has significantly reduced the probability of fractures of hip or vertebra in patients and also aided in the treatment of postmenopausal osteoporosis.[15] All such developments point to the tremendous potential of ST in clinical applications. However, in view that electrical properties of bioceramics have started to mark their presence in clinical settings, the electrical properties of a composite developed from HAP and ST is yet to be considered. Some preliminary studies on the effect of electrical properties (dielectric spectra) of the composite on its biological properties (such as protein adsorption behavior and cytocompatibility) have already been considered in another article.[16] This article primarily focuses on extracting the conduction mechanisms, which (as pointed out earlier) plays a vital role in considering the composites for developing scaffolds and electrets. Another interesting aspect related to the addition of ST derives from the fact that it is an incipient ferroelectric.[17] To improve upon the ϵ_r of a composite, the preferred choice of the monoliths are always ferroelectrics such as $BaTiO_3$, which has been considered for clinical applications as well.[18] However, the drawback associated with ferroelectrics is its remnant polarization, which adversely affects the discharge efficiency that can be detrimental to the performance of electrets. By considering paraelectric like ST, such short-comings can be eliminated along with the possibility of developing composites with high ϵ_r.

Inspired by the exciting developments, this article attempts to explore the conduction mechanisms by fabricating ceramic composite of ST and HAP. We fabricate a series of composites, and their microstructural analysis is reported using X-ray diffraction (XRD). The morphology of the specimens is recorded in a field-emission scanning electron micrograph (FESEM). The specimens are porous, and it may be a result of the insufficient sintering temperature that has been kept low to avoid the formation of other phases of HAP (such as β-tricalcium phosphate). The temperature dependence of conductivity in the composites is studied in the range of 133−523 K. In the chosen temperature range, the conductivity is in the range of ($<10^{-7}$ S/cm), which is relatively low, making it suitable for electret design.[19] Detailed analysis of the conduction mechanism reveals Motts' VRH as the active mechanism (more details on different conduction mechanisms can be found in Figure 1). The hopping energy (W) and the hopping range (R) show a linear variation with temperature. The obtained W is shown to closely relate to the theoretical studies that predict OH^- flipping in the energy range.[20] Finally, a W and R modeling reveals a cubic dependence upon the at. % of ST. The article attempts to present a model for understanding the conduction mechanisms in the bio-ceramic composite as a function of temperature. The range is selected to include the physiological temperature ~310 K, and higher, which would be helpful to predict its usability in the design of bio-electrets. To the best of our knowledge, such mechanisms have never been applied to biomaterials design. It presents a fresh perspective of investigating the biomaterials' suitability by employing the impedance spectroscopy techniques that can be the starting point toward the design and analysis of advanced biomaterials.

■ RESULTS AND DISCUSSION

Microstructural Analysis. The microstructure of the composite specimens is analyzed using the XRD patterns, as shown in Figure 2a. The diffraction patterns confirm the
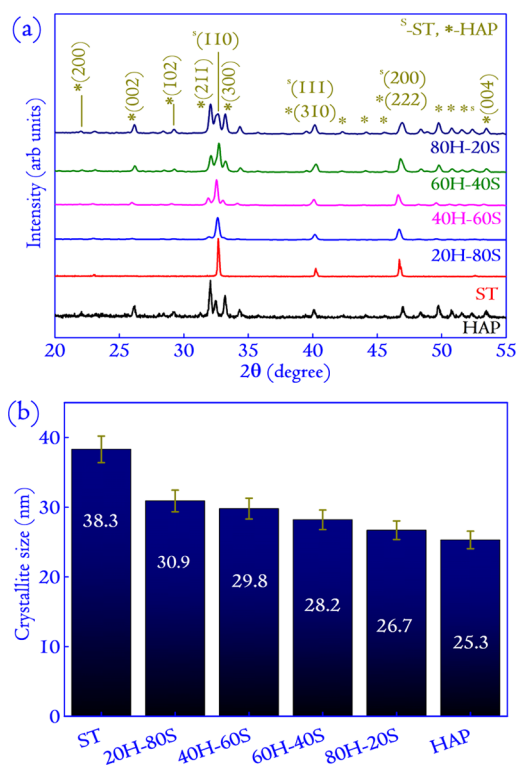
Figure 2. (a) XRD patterns of the composites with varying at. % of ST and HAP. The patterns clearly show reflections corresponding to both the monoliths with some overlaps in certain 2θ position due to the closeness of Braggs' reflection in those positions. No reflections corresponding to reactions between the monoliths are observed in the composites. In (b), the variation in crystallite sizes of the composites determined from the Scherrer formula are plotted. The crystallite size have been calculated using the reflection occurring for the (*hkl*) plane corresponding to the Bragg angle of ~47°.

presence of reflections from both the monoliths. Due to closeness in Bragg reflection positions for the monoliths, certain peaks are seen to undergo a high degree of overlapping. For instance, the (112) reflections at 32.2° for ST overlaps with the (112) reflections of HAP at 32.5° for 80H-20S. Additionally, the XRD pattern shows no trace of a phase that might be formed due to a reaction between the two components of the composites. The crystallite sizes for the composites are evaluated using the Scherrer formula

$$\text{crystallite size } (D) = \frac{k\lambda}{\beta \cos \theta} \quad (1)$$

where k is the Scherrers' constant (0.8−0.9), β denotes the full width at half-maximum in radians, λ denotes the X-ray wavelength, and θ specifies the Bragg angle. The graphical variation in crystallite size is shown in Figure 2b, and it points at systematic dependence with the at. % of ST.[21] Crystallite sizes similar to the present article was also reported by Mobasherpour *et al.*[22] for HAP sintered in the range of 800−900 K. The crystallite size is usually dependent upon the temperature, and with increasing sintering temperature, an enhancement in the crystallite size is observed. In the case of ST, similar values of the crystallite sizes were reported by Sahoo *et al.*[15] It is usually observed that the solid-state processing route is associated with very high sintering temperatures for improved densification of ceramics. This results in larger crystallite sizes of the ST ceramics.[23,24]

The FESEM micrographs of the composite specimens are shown in Figure 3. The grain sizes of the composite specimens are the largest for 20H-80S and decreases with the ST content. For the monoliths, the grain sizes are included in Supporting Information File S1 (Figure S1). As in the crystallite size, the values of grain sizes are found to lie in between the monoliths. ST has a larger grain size, and the HAP (smaller) grains occupy the void spaces between the ST grains. Additionally, the micrographs of the composites are found to have porosity in them. The porosity in the specimens is useful for biological applications.[25] The inherent porosity can regulate the scaffolds' protein adsorption behavior intended to be fabricated from the composites as the porous structures favor protein adsorption. The ceramics' porous nature is due to the lower sintering temperature at which the composites are fired. Traditional firing temperature and soaking time for ceramics are higher than 1273 K, and such high temperatures are responsible for sufficient grain growth.[26] A high sintering temperature provides ample kinetic energy for the grain movement, thereby forcing the particles to the open spaces (porous regions), creating a highly dense structure.[27] The choice of the sintering temperature in the present report is, however, not arbitrary. A high sintering temperature leads to the introduction of phases like β-tricalcium phosphate in HAP.[28] To avoid the transformation, the sintering temperature is fixed at 1073 K. One of the objectives has been to prepare composites with electrical properties to augment the biological properties. A highly dense structure with minimum porosity is desirable for having a very high ϵ_r.[5] Nevertheless, with increased densification, the contact area between the grain increases (due to high-temperature application), contributing to higher conduction, resulting in losses. As pointed out in the Introduction section, such losses will reduce in the magnitude of PEF. Therefore, an optimum density is necessary for composites with sufficiently good electrical properties to compliment the biological response.

Bode Plots. The Bode plots of the composite ceramics determined at 313 K are shown in Figure 4. Bode plots fundamentally represent the frequency dependence of the complex impedance function Z as a function of the frequency f and is defined by the following function

$$Z*(f) = Z'(f) - iZ''(f) \quad (2)$$

where $i = \sqrt{-1}$, $Z'(f) = |Z|\cos\theta$, and $Z''(f) = |Z|\sin\theta$, with $|Z|$ representing the magnitude of the complex impedance function $Z*(f)$. It is clear that $\theta = \arctan(Z''(f)/Z'(f))$. The Bode plot constitutes a plot of Z' versus the frequency f and θ versus the frequency f that helps reveal crucial information about the behavior of the specimens under observation.[29] It is clear from the plots that with increasing frequency, a decrease in the value of $|Z|$ is observed, suggesting an increase in conductivity with increasing frequency. Interestingly, the plot of θ versus f show that, for the most part of the frequency range probed in the article, the value remains close to −90°, implying that the specimens have a capacitive behavior.[29,30] Having understood the nature of the specimens, the next section deals with the conduction mechanisms and their deeper aspects for future biomedical applications.

Conductivity and Hopping Mechanisms. The variation in conductivity of the composites with respect to temperature is shown in Figure 5. From a biomedical perspective, the frequency range of 10^6 to 10^9 Hz [the radio frequency (RF) domain] is used as an effective course of treatment for nonunion of bones and fracture healings.[31] Electrical stimulations
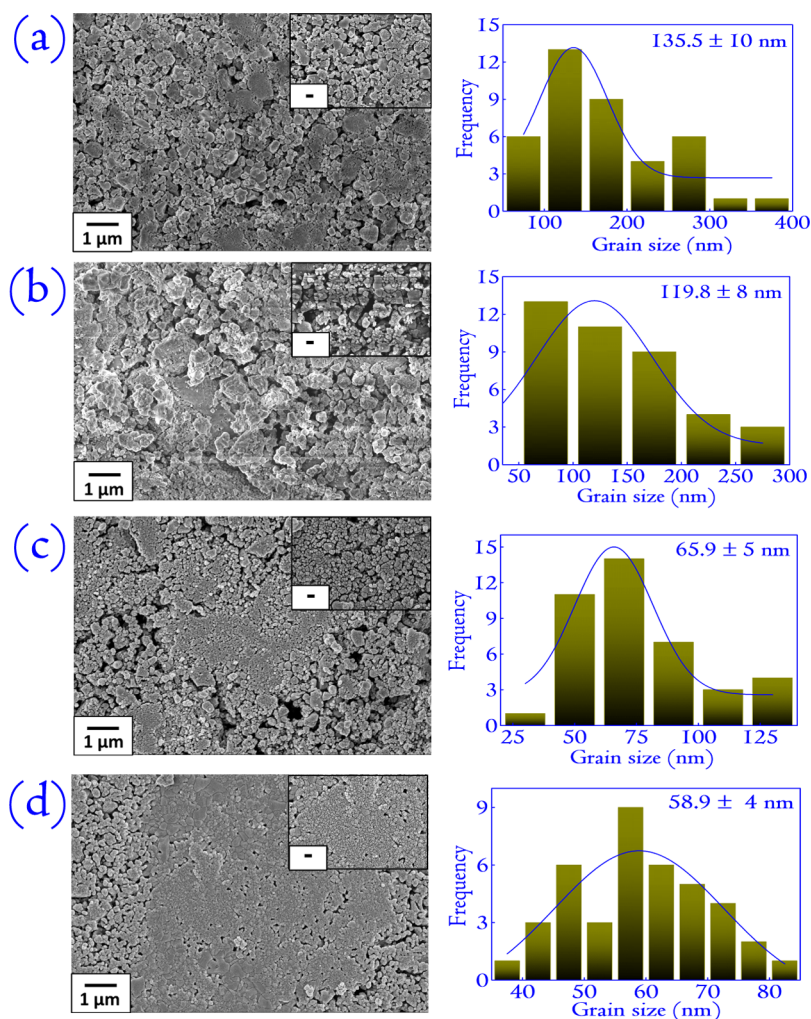
Figure 3. Micrographs of the composites (a) 20H-80S, (b) 40H-60S, (c) 60H-40S, and (d) 80H-20S. In all the micrographs, the porosity is apparent. The porosity in ceramics regulates the physical properties, and in this case, the conductivity. The porosity is also useful from a biological perspective. Inherently porous ceramics are better protein adsorbers and would be suitable as scaffolds for clinical applications. The scale bar in all the magnified figures shown as the inset corresponds to 200 nm.
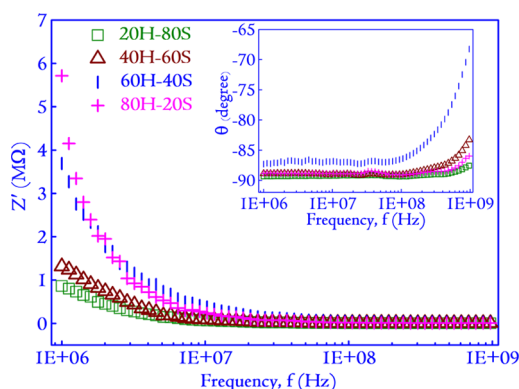

Figure 4. Variation in the real part of impedance with respect to frequency. In the inset, the plot of the phase angle θ vs frequency is shown. The phase angle variation shows that for most of the frequency range, the value remains close to $-90°$, which is an indication of the capacitive behavior of the specimens.

in the form of RF pulses are frequently used for such applications, and although the mechanism is inconclusive, the results are pretty impressive. Biomedical research has hinted at the use of radiofrequency energy to produce superior

hemostasis in bones without any healing complications.[32] Clinicians also have resorted to the use of bipolar RF energy-based devices to avoid necrosis in several applications.[33] It has to be understood that in such applications of RF, the clinicians are yet to arrive at a particular configuration (exact frequency and amplitude of RF that would be suitable for the intended applications).[33] To the best of our knowledge, there is no standard available that determines specific settings of RF for inducing the best healing response.[34] Deriving motivation from such applications, the article is dedicated to understanding the electrical properties (specifically, the behavior of biomaterials to augment the fracture healing process should be understood before their *in vivo* applications). In Figure 5, the conductivity plots show a significant temperature dependence after 300 K when the conductivity rises compared to the dependence at low temperatures. A temperature range of 303−523 K has been chosen for the conductivity analysis primarily for two reasons. The first being incorporation of physiological temperature, at which most of the biophysical reactions take place.[35] Second, the increasing research interest in developing electrets of biomaterials useful in devices like low-powered electrostatic induction generators involves sufficiently high temperatures (310−473 K).[36] Thus, understanding the conduction mech-
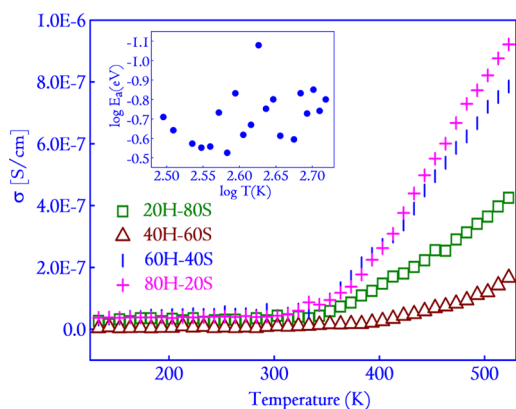
Figure 5. Variations in conductivity with temperature for the composites are plotted. In the inset of the figure, a variation in the E_a with temperature is plotted in log scale to demonstrate the variation in the E_a with temperature for 20H-80S. Also, the variations of conductivity of the specimens with respect to frequency are shown in Figure S2 (Supporting Information File S1) along with the temperature variation of the conductivity of the monoliths, as shown in Figure S3 (Supporting Information File S1). For the other samples, the E_a vs T plot is shown in the Supporting Information File S1 (in Figure S4). In the thermally activated conduction mechanism, E_a remains constant over a specific range of temperature. In the present report, the variation in E_a with temperature points toward the hopping conduction mechanism. The variations are considered in the temperature range of 303−523 K, which is the basis of this report.

anisms is of prime importance in these temperature ranges. A model that describes the conduction process is mathematically formulated as[37]

$$\sigma = \sigma_0 \exp\left(\frac{-E_a}{k_B T}\right) \tag{3}$$

where σ_0 is the pre-exponential factor (a constant), k_B is the Boltzmann constant, T is the temperature, and $E_a = -\frac{d[\ln \sigma]}{d\left[\frac{1}{k_B T}\right]}$ is

the activation energy of bulk conduction specific to the process.[38] The previous expressions' versatility lies in its ability to determine the E_a of the conduction process irrespective of the mechanism active within the specimens'. At non-zero temperatures, specifically in insulators like bioceramics, the free carriers' concentration is close to nil. The density of defects, impurities, and trapping centers for the electrons is typically higher. Therefore, hopping is the main conduction mechanism until the room temperature and even higher.[39] There are two types of hopping mechanisms relevant to bioceramics, namely, the nearest-neighbor hopping conduction (NNH) and the VRH conduction. In the NNH mechanism, the hopping takes place to the nearest neighboring empty sites, and in literature, it is cited that the E_a of such conduction process must be valued constantly for a particular range.[40] However, it is clear from the inset of Figure 5 that E_a is a temperature-dependent function. The variable nature of E_a is an indication of the existence of VRH mechanisms in the specimens, consistent with the VRH theory.

Understanding the hopping mechanism from the perspective of resistivity ($\rho = (1/\sigma)$) can reveal a plethora of information about the mechanism of conduction within the specimens'. The conclusions extracted from resistivity or conductivity plots equally apply even if conductivity instead of resistivity is chosen for analysis. In the VRH process, the charge carriers

hop between levels close to the Fermi level without dependence on their spatial distribution.[41] Unlike NNH, the VRH process is categorized by the variable hopping distance. Two types of VRH are defined in literature, namely, the Efros−Shklovskii (ES-VRH) and the Motts' 3D VRH. The following equations can appropriately describe the models[34]

$$\rho = \rho_0 \exp\left(\frac{T_0}{T}\right)^p \tag{4}$$

where ρ_0 is the pre-exponential factor ($\rho_0 = 1/\sigma_0$, a constant), T_0 is the characteristic temperature relevant to the prevalent conduction mechanism, and $p = 1/2$ or $1/4$, respectively, depending on the form of density of states (DOS) at the Fermi level. In disordered systems without Coulomb interactions, $p = 1/4$ leads to the Motts' VRH mechanism that thrives on the assumption that the DOS remains constant near the Fermi level.[42−44] The ES-VRH model is derived by considering $p = 1/2$, and it justifies the existence of Coulomb interaction between the initial and final hopping states for the long-range electron hopping.[42] In this model, there is a quadratic diminishing of the DOS near the Fermi level. Identifying the dominant conduction mechanism from a diverse set of available models largely depends on fitting the appropriate model to the conductivity/resistivity data. The choice between $p = 1/2$ or $1/4$ is typically made by fitting the above eq 4 with different values of p. The value of p that best fits the equation gives the dominant conduction mechanism in the probed temperature range. However, fitting the model with different values of p is quite a tedious task, and instead, we adopt a different approach by considering a slight modification of eq 4

$$\ln[\ln(\rho) - \ln(\rho_0)] = p[\ln(T_0) - \ln(T)] \tag{5}$$

which is an equation of the form $y = mx + c$, with $m = -p$, $y = \ln[\ln(\rho/\rho_0)]$ and $x = \ln(T)$. The mathematical manipulation provides us with the straight-line slope to determine the nature of the conduction mechanism active within the specimens. These variations are shown in Figure 6a. In all the composites, the slopes are close to $1/4$, suggesting Motts' VRH to be the dominant mechanism in the specimens (in the considered temperature range). A plot of the linear fitting is shown in the inset of Figure 6a, and the other linear fits are shown in Supporting Information File S1 (Figure S5). This determination of p is identified as the Zabrodskii analysis and is an unbiased and quantitative method of identifying the conduction mechanism.[45] In all the cases, the linear fit of $\ln[\rho]$ versus $T^{-1/4}$ [see Figure 6b and Supporting Information File S1 (Figure S6)] matches the experimental data quite appropriately with the adj. R^2 value in each of the plots is greater than 0.9. It again confirms the fact that Motts' VRH mechanism can describe the data more satisfactorily in the chosen temperature range.

It is stated earlier that T_0 in eq 4 and hence eq 5 is the characteristic temperature dependent upon the active conduction mechanism in the specimen. Incidentally, the parameter T_0 forms an important quantity in the determination of DOS near the Fermi level $N(E_F)$.[45] The easiest way to extract T_0 is by making a plot of $\ln[\rho]$ versus $T^{-1/4}$, which ought to be straight line (see eq 6). The value of T_0 is inversely proportional to the DOS that can be extracted using the following equation[36]
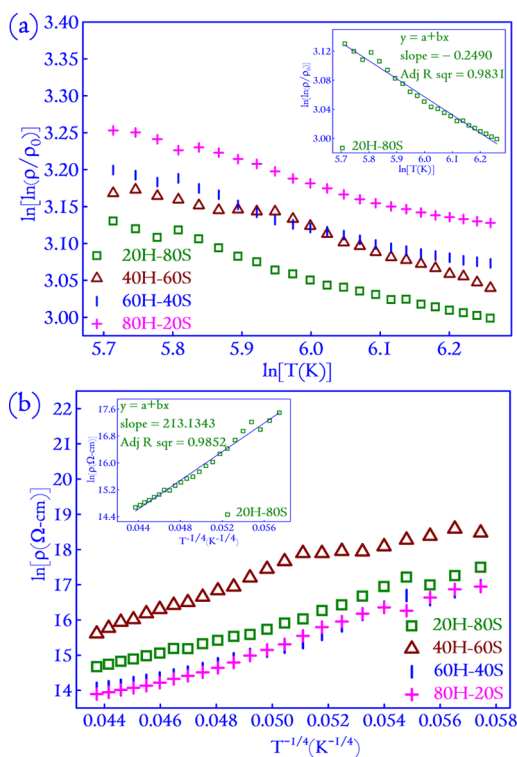
Figure 6. (a) Plot of $\ln[\ln(\rho/\rho_0)]$ *vs* $\ln[T]$ that helps to identify the VRH mechanism in the composite in a temperature range of 303−523 K. The slope of all the linear fits are close to 0.25, and this value identifies the Motts' VRH mechanism to be the dominant conduction mechanism in the ceramic composites'. For brevity, the linear fit is shown only for 20H-80S. The other plots have been included in Supporting Information File S1 (Figure S5). (b) Plot of $\ln[\rho]$ *vs* $T^{-1/4}$, which enables to calculate the DOS that is intrinsic to the Motts' VRH mechanism. For brevity, the linear fit is considered only for 20H-80S, including the others in the Supporting Information File S1 (Figure S6).

$$\rho = \rho_0 \exp\left(\frac{T_0}{T}\right)^{1/4} \tag{6}$$

$$N(E_F) = \frac{16}{T_0 k_B \zeta^3} \tag{7}$$

where ζ $(=\alpha^{-1})$ is the decay length of the localized wave function and signifies the spatial extension of the wave function $(e^{-\alpha R})$ associated to the localized states (R denoting the hopping length). There is a dearth of literature on the value of ζ for the chosen composite. Deriving from the case of $BaTiO_3$, ζ is considered to be approximately 0.40 nm.[36,37] This particular value is chosen for calculation of $N(E_F)$ using eq 7. The calculated values are 3.51×10^{19}, 2.81×10^{19}, 2.66×10^{19}, and 2.12×10^{19} for 20H-80S, 40H-60S, 60H-40S, and 80H-20S, respectively. Finishing the discussion, two critical parameters, namely, the hopping length (R) and the hopping energy (W) are determined from the Motts' VRH model using the following equations.[38]

$$R = \frac{3}{4}\left[\frac{3\zeta}{2\pi N(E_F)k_B T}\right]^{1/4} \text{ and } W = \left[\frac{3}{4\pi R^3 N(E_F)}\right] \tag{8}$$

The values calculated for R and W are shown as a function of temperature T in Figure 7. For all the composites, the value of
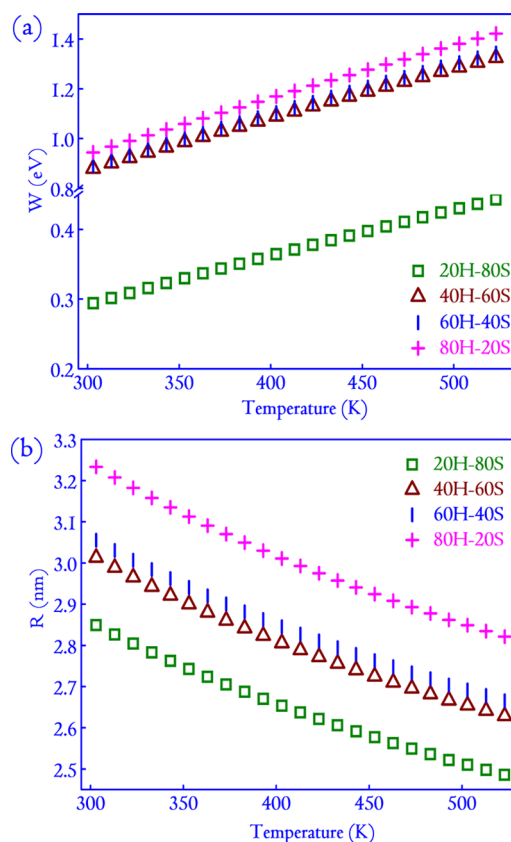

Figure 7. (a) Variation of the hopping length R and (b) hopping energy W as a function of temperature. R and W shows a linear variation, W increases linearly as a function of temperature, and R decreases linearly.

R and W show a linear variation with temperature T.[45] Also, the essential conditions $W \geq k_B T$ and $R/\zeta \geq 1$ are satisfied in all the cases by the ceramic composites that confirm the validity of the approach. The calculated values of the parameters associated to R and W along with the DOS are shown in Table 1. To analyze the evolution of R and W at 310

Table 1. Variation of the DOS for Various Specimens and Verification of the Essential Conditions $W \geq k_B T$ and $R/\zeta \geq 1$ at 310 K[a]

sample	$N(E_F)$ $(eV^{-1})(cm^{-3})$	W	R/ζ
20H-80S	3.51×10^{19}	0.30	2.83
40H-60S	2.81×10^{19}	0.32	2.99
60H-40S	2.66×10^{19}	0.32	3.04
80H-20S	2.12×10^{19}	0.34	3.21

[a]At 310 K, the value of $k_B T$ is 0.026110, which is lesser than all the tabulated values of W. Also in all the cases, R/ζ is greater than 1 (where ζ is assumed to be 0.40 nm).

K due to ST addition to HAP, a plot is made, and the variations are shown in Figure 8. In both cases, the variation is appropriately fitted with a cubic polynomial with the fitted parameters appropriately represented in Figure 8.

■ DISCUSSION

The electrical properties of biomaterials present the new hotspot of biomedical research. Biomaterials with exquisite properties like piezoelectricity and ferroelectricity have been
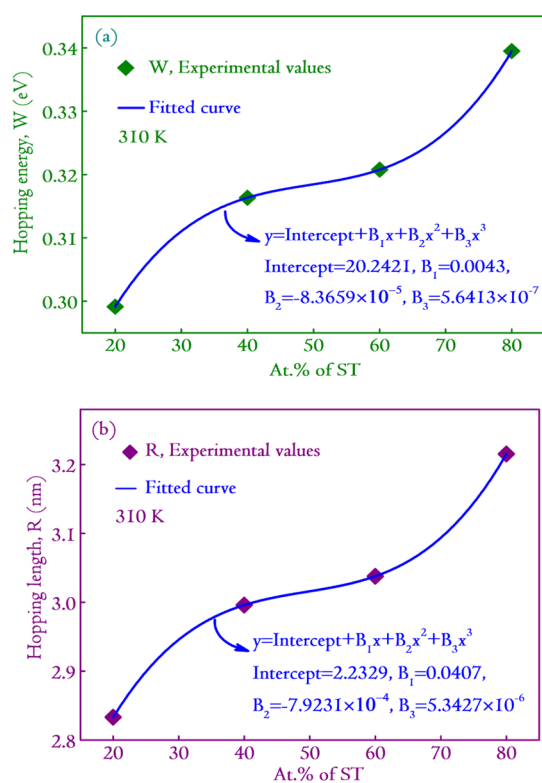
Figure 8. (a,b) Variation of the hopping length R and hopping energy W at 310 K. The variations are plotted against the at. % of ST for the ceramic composites. The variation is best fitted with a cubic polynomial function with the parameters demonstrated appropriately in the figure legend.

considered the next generation of smart biomaterials that hold potential for faster wound recovery and improved biological response.[46,47] Natural bones are electrically active under the effect of mechanical loading due to the presence of collagen.[48] Inspired by natural design, the integration of electrically active artificial implants to injured sites has been considered by the biomaterials research community. Many phenomena related to the electrical properties of natural bones are yet to be fully understood. This inspired us to investigate a composite material that has shown promising biological properties from the elegant formalism of impedance spectroscopy, with a particular focus on the loss mechanisms. Designing an electrically active biomaterial would naturally require analyzing its electrical properties comprehensively. For instance, after implanting a scaffold, the electrical stimulation periodically will lead to faster bone regeneration.[36,48] When subjected to electric fields, it is well known that dielectrics would undergo dipolar polarization, which gradually dies out after removing the external field.[5] The rate at which the polarization dies down depends on the loss mechanism (specifically the conduction) active within the dielectrics. In alternating fields, the dielectrics undergo dipolar relaxation (a phenomenon related to the decrease in the ϵ_r due to the dipoles' inability to follow the variations in the frequency of the external field).[5,49] Therefore, to effectively make use of the PEF in *in vivo* settings, the frequency of the external field must be tuned to extract the maximum polarization field of the dielectric. Then, even after removing the external field, the scaffold would keep generating the PEF, which will continue augmenting the expedited healing process. However, the articles' theme is not to measure the

PEF; instead, we show the adaption of the established formalism of the conduction mechanism to understand the physical properties of the biomaterials system. Notable few mentions where such properties can be useful are the biomaterials' applications to design bio-electronic gadgets and electrically active implantable medical devices with stimulation capabilities (Table 1).

Interesting properties emerge when one applies the established VRH mechanisms to bio-ceramic composites. Motts' VRH mechanism is an interesting phenomenon and is already applied to ceramic composites such as that of $Bi_{0.5}Na_{0.5}TiO_3-K_{0.5}Na_{0.5}NbO_3$ in the temperature range of 300−419 and 562−589 K.[31] The values of W, as well as R, are found to be similar to the present case. Interestingly, it is pointed out that the polarization mechanisms active within HAP specimens, especially in the activation energy domain of 0.2−0.8 eV, relate to OH flipping in HAP and are consistent with the range of hopping energy in ceramics.[37] It points to a close correlation between the active conduction mechanisms and the polarization mechanisms in ceramics. In ST, a transition metal oxide, usually the oxygen vacancies, is naturally formed at the high-temperature sintering process (∼1073 K). In the temperature window, the oxygen vacancies are reported to be in a doubly positive charged state (at and above 800 K). Below 800 K, the doubly positive charged state changes to the singly ionized state by absorbing an electron. We believe that the vacancies provide a platform for the charge carriers to hop along, thereby contributing to the polarization mechanisms in ST.[50] For exhibiting lesser conduction, the hopping motion of the dipoles is highly localized to the lattice. This would prevent the hopping dipoles from establishing a long-range ordering in the composite materials. From Figure 7, it can be inferred that the hopping distance in the composites is relatively short in comparison to many other reports.[22,24]

■ CONCLUSIONS

Our study broadens the scope of established conduction mechanisms from conventional ceramics to inherently different bio-ceramic composites. By microstructural analysis, we establish that the ceramic composite individually contains signatures of both the monoliths. No trace of a phase due to reaction between the monoliths is found. The crystallite size and the grain size increased with an increase in the at. % of ST. The FESEM micrographs revealed that the composites are porous. The Bode plots reveal that the specimens have a capacitive behavior for most part of the frequency range probed in the experiment. The article points at an interesting association of the service lifetime of electrets and the active conduction mechanisms. We remark that the lower conductivity ($\simeq 10^{-8}$ S/cm) can serve as an indirect way for estimation of the service life. Also, the lower conductivity is associated with the inherently porous nature of the specimens, which reduces the effective contact area between the grains, and thus reducing the conductivity drastically. Theoretical advances in the study of electrical properties (specifically in the field of conductivity mechanisms) are yet to be rigorously considered in the design of bio-electrets. The article will serve to bridge the gap between theory and industry. A ceramic composite of HAP and ST, specifically for electrets, can be a strong starting point in this direction. The results established in the article can be beneficial for designing prototype electrets and scaffolds in biomedical applications.

■ MATERIALS AND METHODS

Specimen Preparation. A series of ceramic composites by mixing HAP and ST in different at. % (the nomenclature and exact compositions included in Table 2) is prepared for the

Table 2. Composition of Different Green Discs and Their Codes

1st	2nd	mixing ratio	codes
HAP	ST	100 at. % HAP	HAP
		20 at. % HAP & 80 at. % ST	20H-80S
		40 at. % HAP & 60 at. % ST	40H-60S
		60 at. % HAP & 40 at. % ST	60H-40S
		80 at. % HAP & 20 at. % ST	80H-20S
		100 at. % ST	ST

study. The monolith HAP is prepared from $Ca(NO_3)_2 \cdot 4H_2O$ and P_2O_5 (all procured from Sigma-Aldrich, USA) precursors using the sol–gel route. Specifically, two beakers containing 25 mL of ethanol are continuously stirred over two magnetic stirrers (Tarsons, India) when the two precursors (measured in the molar ratio 10:6) are added to it. To ensure that the precursors undergo complete dissolution, the stirring is done for 30 min, after which the individual solutions are mixed. During mixing, there should not be any precipitation in the solution. This is ensured by adding one solution to the other dropwise. Once the mixing is complete, the final reaction mixture is allowed to undergo stirring for 24 h for a complete dissolution of the solution mixture. It is followed by 24 h of aging, during which the stirring is stopped, and the solution is kept undistrubed. During the period, the solution mixture transforms into a dense gel, which is dried in an oven (Optics Technology, India) at 363 K overnight. The process of drying transforms the gel into powder. The powder is finally calcined in a conventional furnace (Nabertherm, Germany) at 773 K for 2 h to obtain phase pure HAP powder.

To obtain ST, the precursors weighed according to stoichiometry (refer eq 9) are mixed in a planetary ball mill (PULVERISETTE 6, Fritsch, Germany) using propanol as the grinding media in a Zirconia jar. $SrCO_3$ and TiO_2 are used as the precursors (all procured from Sigma-Aldrich, USA) for producing $SrTiO_3$. The initial precursors are mixed by following the reaction

$$SrCO_3 + TiO_2 \rightarrow SrTiO_3 + CO_2\uparrow \tag{9}$$
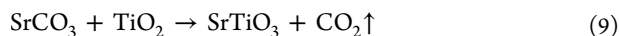
The contents are ball-milled at 250 rpm for 5 h (maintaining the ball and powder ratio at 10:1). A thick slurry is formed at the end of the reaction, which is transferred into a glass beaker for drying at 363 K in a hot air oven. Once the drying is complete, the remnants (in powder form) are transferred into alumina crucibles and are calcined at 1473 K for 4 h. For preparing the composites, the monoliths are mixed according to their stoichiometry (as shown in Table 2) in a ball mill using the procedure described above. The composite slurry recovered after ball milling is dried, and the powder is considered for making green discs. The poly-vinyl alcohol (Loba Chemie, India) which acts as the composites' binding agent is thoroughly mixed with the composite powder, and the powder is pressed in a hydraullic press (Technosearch, India) at 25 kg/cm². These green discs are finally fired in a hot air furnace at 1073 K for achieving compaction. Following compaction, the discs (thickness ~1 mm and diameter ~10 mm) are converted to metal–insulator–metal (MIM)

capacitors by coating silver paste (Sigma-Aldrich, USA) on both sides of the discs, similar to electrets.

Characterization. The phase composition and the microstructure of the compact discs are analyzed using an X-ray diffractometer (Rigaku, TTRAX III, Japan). The diffraction patterns are recorded for Braggs' angle of 20−55°, scanning the specimens at 3°/min and collecting the X-ray photons at a step size of 0.03°. The diffractometer uses Cu Kα radiation of wavelength 1.5406 Å. The FESEM (Sigma Zeiss, Germany) images are recorded to observe the morphology of the composite specimens and determining their grain sizes. The grain sizes are measured by using the ImageJ software. For measuring the conductivity, an impedance analyzer (Agilent Technologies 4991A, USA) is used, where the fabricated MIM capacitors are loaded into a sample holder. By varying the frequency in the range of 1 MHz to 1 GHz, the data for the conductivity of the specimens are collected. The temperature variation of the specimens for a wide range starting from 133 to 523 K is carried out using a temperature controller (Novocontrol, Germany) setup linked with the impedance analyzer. The temperature controller uses liquid N_2 for temperature control, and the frequency sweep was done after the temperature stabilized at an interval of 10 K each (starting from 133 K).

■ ASSOCIATED CONTENT

Ⓢ Supporting Information

The Supporting Information is available free of charge at https://pubs.acs.org/doi/10.1021/acsomega.1c02273.

> FESEM micrographs of the monoliths with the top row representing the ST and the bottom row representing HAP; variation in the conductivity of the specimens with respect to frequency (1 MHz to 1 GHz); zoomed-in view of the conductivity variation; variation of conductivity with respect to frequency for the monoliths HAP and ST; variation in the conductivity of the monoliths at 1 MHz with respect to temperature; variation in the values of E_a with temperature; linear fit in the plot of $\ln[\ln(\rho/\rho_0)]$ versus $\ln T$ for 40H-60S, 60H-40S, and 80H-20S, respectively; linear fit in the plot of $\ln[\rho]$ versus $T^{-1/4}$ for 40H-60S, 60H-40S, and 80H-20S, respectively (PDF)

■ AUTHOR INFORMATION

Corresponding Author

Pamu Dobbidi − *Department of Physics, Indian Institute of Technology Guwahati, Guwahati 781039 Assam, India;* ⓞ orcid.org/0000-0002-0834-8461; Email: pamu@ iitg.ac.in

Author

Apurba Das − *Department of Physics, Indian Institute of Technology Guwahati, Guwahati 781039 Assam, India*

Complete contact information is available at:
https://pubs.acs.org/10.1021/acsomega.1c02273

Notes

The authors declare no competing financial interest.

■ ACKNOWLEDGMENTS

■ REFERENCES

(1) Rajabi, A. H.; Jaffe, M.; Arinzeh, T. L. Piezoelectric materials for tissue regeneration: A review. *Acta Biomater.* **2015**, *24*, 12.

(2) Thakral, G.; LaFontaine, J.; Najafi, B.; Talal, T. K.; Kim, P.; Lavery, L. A. Electrical stimulation to accelerate wound healing. *Diabet. Foot Ankle* **2013**, *4*, 22081.

(3) Fallahiarezoudar, E.; Ahmadipourroudposht, M.; Idris, A.; Mohd Yusof, N. A review of: Application of synthetic scaffold in tissue engineering heart valves. *Mater. Sci. Eng., C* **2015**, *48*, 556.

(4) Tandon, B.; Blaker, J. J.; Cartmell, S. H. Piezoelectric materials as stimulatory biomedical materials and scaffolds for bone repair. *Acta Biomater.* **2018**, *73*, 1.

(5) Kao, K. C. *Dielectric Phenomena in Solids*, 1st ed.; Elsevier Academic Press, 2004; pp 41−114.

(6) Chiu, F.-C. Review on Conduction Mechanisms in Dielectric Films. *Adv. Mater. Sci. Eng.* **2014**, *2014*, 1.

(7) Das, A.; Dobbidi, P. Impedance Spectroscopy and ac Conductivity in $Ba_{0.5}Sr_{0.5}TiO_3-Ca_{10}(PO_4)_6(OH)_2$ Ceramic Composites: An Electrical Approach to Unveil Biocomposites. *ACS Biomater. Sci. Eng.* **2021**, *7*, 2296.

(8) Bhogra, A.; Masarrat, A.; Meena, R.; Hasina, D.; Bala, M.; Dong, C.-L.; Chen, C.-L.; Som, T.; Kumar, A.; Kandasami, A. Tuning the Electrical and Thermoelectric Properties of N Ion Implanted $SrTiO_3$ Thin Films and Their Conduction Mechanisms. *Sci. Rep.* **2019**, *9*, 14486.

(9) Tandon, B.; Magaz, A.; Balint, R.; Blaker, J. J.; Cartmell, S. H. Electroactive biomaterials: Vehicles for controlled delivery of therapeutic agents for drug delivery and tissue regeneration. *Adv. Drug Delivery Rev.* **2018**, *129*, 148.

(10) Horiuchi, N.; Madokoro, K.; Nozaki, K.; Nakamura, M.; Katayama, K.; Nagai, A.; Yamashita, K. Electrical conductivity of polycrystalline hydroxyapatite and its application to electret formation. *Solid State Ionics* **2018**, *315*, 19.

(11) Yamashita, K. *Electrically Active Materials for Medical Devices*, 1st ed.; World Scientific, 2016; pp 91−102.

(12) Lang, S. B.; Tofail, S. A. M.; Kholkin, A. L.; Wojtaś, M.; Gregor, M.; Gandhi, A. A.; Wang, Y.; Bauer, S.; Krause, M.; Plecenik, A. Ferroelectric Polarization in Nanocrystalline Hydroxyapatite Thin Films on Silicon. *Sci. Rep.* **2013**, *3*, 2215.

(13) Xin, Y.; Jiang, J.; Huo, K.; Hu, T.; Chu, P. K. Bioactive $SrTiO_3$ Nanotube Arrays: Strontium Delivery Platform on Ti-Based Osteoporotic Bone Implants. *ACS Nano* **2009**, *3*, 3228.

(14) Wang, Y.; Zhang, D.; Wen, C.; Li, Y. Processing and Characterization of $SrTiO_3-TiO_2$ Nanoparticle Nanotube Heterostructures on Titanium for Biomedical Applications. *ACS Appl. Mater. Interfaces* **2015**, *7*, 16018.

(15) Sahoo, S.; Sinha, A.; Das, M. Synthesis, characterization and in vitro biocompatibility study of strontium titanate ceramic: A potential biomaterial. *J. Mech. Behav. Biomed. Mater.* **2020**, *102*, 103494.

(16) Das, A.; Bhardwaj, A.; Rabha, S.; Pandey, L. M.; Pamu, D. Physical, chemical and biological investigations of $SrTiO_3-Ca_{10}(PO_4)_6(OH)_2$ composites for biomedical applications. *J. Am. Ceram. Soc.* **2021**, DOI: 10.1111/jace.17952.

(17) Zhang, H.; Zhu, Y.; Li, Z.; Fan, P.; Ma, W.; Xie, B. High discharged energy density of polymer nanocomposites containing paraelectric $SrTiO_3$ nanowires for flexible energy storage device. *J. Alloys Compd.* **2018**, *744*, 116.

(18) Das, A.; Pamu, D. A comprehensive review on electrical properties of hydroxyapatite based ceramic composites. *Mater. Sci. Eng., C* **2019**, *101*, 539.

(19) Gross, B. Experiments on Electrets. *Phys. Rev.* **1944**, *66*, 26.

(20) Kasamatsu, S.; Sugino, O. First-principles investigation of polarization and ion conduction mechanisms in hydroxyapatite. *Phys. Chem. Chem. Phys.* **2018**, *20*, 8744.

(21) Li, Q.; Kartikowati, C. W.; Horie, S.; Ogi, T.; Iwaki, T.; Okuyama, K. Correlation between particle size/domain structure and magnetic properties of highly crystalline Fe_3O_4 nanoparticles. *Sci. Rep.* **2017**, *7*, 9894.

(22) Mobasherpour, I.; Heshajin, M. S.; Kazemzadeh, A.; Zakeri, M. Synthesis of nanocrystalline hydroxyapatite by using precipitation method. *J. Alloys Compd.* **2007**, *430*, 330.

(23) Klaytae, T.; Panthong, P.; Thountom, S. Preparation of nanocrystalline $SrTiO_3$ powder by sol-gel combustion method. *Ceram. Int.* **2013**, *39*, S405.

(24) Chang, C.-H.; Shen, Y.-H. Synthesis and characterization of chromium doped $SrTiO_3$ photocatalyst. *Mater. Lett.* **2006**, *60*, 129.

(25) Saikia, J.; Yazdimamaghani, M.; Hadipour Moghaddam, S. P.; Ghandehari, H. Differential Protein Adsorption and Cellular Uptake of Silica Nanoparticles Based on Size and Porosity. *ACS Appl. Mater. Interfaces* **2016**, *8*, 34820.

(26) Arbatti, M.; Shan, X.; Cheng, Z.-Y. Ceramic-polymer composites with high dielectric constant. *Adv. Mater.* **2007**, *19*, 1369.

(27) Waser, R.; Hagenbeck, R. Grain boundaries in dielectric and mixed-conducting ceramics. *Acta Mater.* **2000**, *48*, 797.

(28) Yousefi, A.-M.; Oudadesse, H.; Akbarzadeh, R.; Wers, E.; Lucas-Girot, A. Physical and biological characteristics of nano-hydroxyapatite and bioactive glasses used for bone tissue engineering. *Nanotechnol. Rev.* **2014**, *3*, 527.

(29) Bouvet, G.; Nguyen, D. D.; Mallarino, S.; Touzain, S. Analysis of the non-ideal capacitive behaviour for high impedance organic coatings. *Prog. Org. Coat.* **2014**, *77*, 2045.

(30) Price, D. T. *MEMS for Biomedical Applications*, 1st ed.; Woodhead Publishing, 2012; pp 97−119.

(31) Menendez, M.; Ishihara, A.; Weisbrode, S.; Bertone, A. Radiofrequency energy on cortical bone and soft tissue: A pilot study. *Clin. Orthop. Relat. Res.* **2010**, *468*, 1157.

(32) Bertone, A.; Lipson, D.; Kamei, J.; Litsky, A.; Weisbrode, S. Effective bone hemostasis and healing using radiofrequency and conductive fluid. *Clin. Orthop. Relat. Res.* **2006**, *446*, 278.

(33) Goldstein, C.; Sprague, S.; Petrisor, B. A. Electrical Stimulation for Fracture Healing: Current Evidence. *J. Orthop. Trauma* **2010**, *24*, S62.

(34) Griffin, M.; Bayat, A. Electrical stimulation in bone healing: critical analysis by evaluating levels of evidence. *Eplasty* **2011**, *11*, No. e34.

(35) Sarma, B. K.; Das, A.; Barman, P.; Pal, A. R. Biomimetic growth and substrate dependent mechanical properties of bone like apatite nucleated on Ti and magnetron sputtered TiO_2 nanostructure. *J. Phys. D: Appl. Phys.* **2016**, *49*, 145304.

(36) Han, H.; Davis, C., III; Nino, J. C. Variable Range Hopping Conduction in $BaTiO_3$ Ceramics Exhibiting Colossal Permittivity. *J. Phys. Chem. C* **2014**, *118*, 9137.

(37) Wada, N.; Horiuchi, N.; Mukougawa, K.; Nozaki, K.; Nakamura, M.; Nagai, A.; Okura, T.; Yamashita, K. Electrostatic induction power generator using hydroxyapatite ceramic electrets. *Mater. Res. Bull.* **2016**, *74*, 50.

(38) Zubair Ansari, M.; Khare, N. Thermally activated band conduction and variable range hopping conduction in Cu_2ZnSnS_4 thin films. *J. Appl. Phys.* **2015**, *117*, 025706.

(39) Shlimak, I. *Is Hopping a Science?*, 1st ed.; World Scientific, 2015; pp 1−18.

(40) Pattipaka, S.; James, A. R.; Dobbidi, P. Enhanced dielectric and piezoelectric properties of BNT-KNNG piezoelectric ceramics. *J. Alloys Compd.* **2018**, *765*, 1195.

(41) Lin, T. T.; Young, S. L.; Kung, C. Y.; Chen, H. Z.; Kao, M. C.; Chang, M. C.; Ou, C. R. Variable-Range Hopping and Thermal Activation Conduction of Y-Doped ZnO Nanocrystalline Films. *IEEE Trans. Nanotechnol.* **2014**, *13*, 425.

(42) Hu, T.; Shklovskii, B. I. Theory of hopping conductivity of a suspension of nanowires in an insulator. *Phys. Rev. B: Condens. Matter Mater. Phys.* **2006**, *74*, 054205.

(43) Somoza, A. M.; Ortuno, M.; Pollak, M. Collective variable-range hopping in the Coulomb gap: Computer simulations. *Phys. Rev. B: Condens. Matter Mater. Phys.* **2006**, *73*, 045123.

(44) Zabrodskii, A. G.; Zinoveva, K. N. Critical behavior of N-Ge parameters in the region of compensation-induced Anderson transition. *JETP Lett.* **1983**, *37*, 436.

(45) Pattipaka, S.; Peddigari, M.; Dobbidi, P. Dielectric and ferroelectric properties of Gd^{3+} doped $(K_{0.5}Na_{0.5})_{0.96}Li_{0.04}(Nb_{0.8}Ta_{0.20})O_3$ piezoelectric ceramics. *Mater. Sci. Eng., B* **2020**, *252*, 114470.

(46) Blázquez-Castro, A.; García-Cabañes, A.; Carrascosa, M. Biological applications of ferroelectric materials. *Appl. Phys. Rev.* **2018**, *5*, 041101.

(47) Minary-Jolandan, M.; Yu, M.-F. Uncovering Nanoscale Electromechanical Heterogeneity in the Subfibrillar Structure of Collagen Fibrils Responsible for the Piezoelectricity of Bone. *ACS Nano* **2009**, *3*, 1859.

(48) Leppik, L. P.; Froemel, D.; Slavici, A.; Ovadia, Z. N.; Hudak, L.; Henrich, D.; Marzi, I.; Barker, J. H. Effects of electrical stimulation on rat limb regeneration, a new look at an old model. *Sci. Rep.* **2016**, *5*, 18353.

(49) Gittings, J. P.; Bowen, C. R.; Dent, A. C. E.; Turner, I. G.; Baxter, F. R.; Chaudhuri, J. B. Electrical characterization of hydroxyapatite-based bioceramics. *Acta Biomater.* **2009**, *5*, 743.

(50) Wang, C. C.; Lei, C. M.; Wang, G. J.; Sun, X. H.; Li, T.; Huang, S. G.; Wang, H.; Li, Y. D. Oxygen-vacancy-related dielectric relaxations in $SrTiO_3$ at high temperatures. *J. Appl. Phys.* **2013**, *113*, 094103.